Vibrational Strong Coupling

How to cite:
International Edition: doi.org/10.1002/anie.202103920
German Edition: doi.org/10.1002/ange.202103920

Collective Vibrational Strong Coupling Effects on Molecular Vibrational Relaxation and Energy Transfer: Numerical Insights via Cavity Molecular Dynamics Simulations**

Tao E. Li, Abraham Nitzan,* and Joseph E. Subotnik**

Abstract: *For a small fraction of hot CO_2 molecules immersed in a liquid-phase CO_2 thermal bath, classical cavity molecular dynamics simulations show that forming collective vibrational strong coupling (VSC) between the C=O asymmetric stretch of CO_2 molecules and a cavity mode accelerates hot-molecule relaxation. This acceleration stems from the fact that polaritons can be transiently excited during the nonequilibrium process, which facilitates intermolecular vibrational energy transfer. The VSC effects on these rates 1) resonantly depend on the cavity mode detuning, 2) cooperatively depend on Rabi splitting, and 3) collectively scale with the number of hot molecules. For larger cavity volumes, the average VSC effect per molecule can remain meaningful for up to $N \approx 10^4$ molecules forming VSC. Moreover, the transiently excited lower polariton prefers to relax by transferring its energy to the tail of the molecular energy distribution rather than distributing it equally to all thermal molecules. As far as the parameter dependence is concerned, the vibrational relaxation data presented here appear analogous to VSC catalysis in Fabry–Pérot microcavities.*

Introduction

Collective vibrational strong coupling (VSC) can occur if a macroscopic number of liquid-phase molecules are confined to a Fabry–Pérot microcavity and a molecular vibrational mode is near resonant with a cavity mode.[1,2] Under collective VSC, experimental reports indicate not only a peak splitting, i.e., a Rabi splitting within molecular infrared (IR) spectroscopy, but also the modification of chemical reaction rates[3–6] and crystallization processes[7] under thermal conditions. As pioneered first by Ebbesen[3] and co-workers, these observations suggest that collective VSC might meaningfully modify individual molecular properties *without* external pumping—although these intriguing experimental findings cannot yet be well explained by current theory.[8–13]

A simple example illustrating how conventional theory fails to explain the Ebbesen experiments is to consider the case of N molecules forming VSC with a Rabi splitting $\Omega_N = 2g_0\sqrt{N} \approx 100\ \mathrm{cm}^{-1}$, where g_0 denotes the light-matter coupling for individual molecules. Because g_0 $(=\Omega_N/2\sqrt{N})$ is negligible when N becomes macroscopic, one would guess that individual molecular properties (such as chemical reaction rates) cannot be meaningfully modified by a Fabry–Pérot microcavity, a theoretical prediction at odds with several experiments. Recent efforts[10,14] also suggest that, within a classical description of cavity photons and molecules, static properties of individual molecules during thermal equilibrium are entirely unchanged under usual VSC setups, indicating a nonequilibrium (or perhaps quantum) origin of the Ebbesen experiments.

In order to narrow the gap between theory and experiment, here we numerically investigate VSC effects on two nonequilibrium processes—molecular vibrational energy relaxation and intermolecular vibrational energy transfer. These vibrational processes have been extensively studied both experimentally and theoretically outside a cavity, and the rates of which have been known to play an important role in many physical and chemical processes, including chemical reactions.[15] Ref. [16] has studied the effect of VSC on intermolecular vibrational energy transfer rates by quantifying the response of hybrid light-matter states (polaritons) after pumping the upper polariton (UP) for a liquid mixture of $W(^{12}CO)_6$ and $W(^{13}CO)_6$.

For the sake of simplicity, here our numerical study focuses on a pure liquid CO_2 system when the C=O asymmetric stretch forms VSC with a single optical cavity mode (where two polarization directions are included). In such a system, instead of exciting polaritons, we will consider the case when a small fraction of uncorrelated hot CO_2 molecules dissipates and transfers vibrational energy to the remaining thermal CO_2 molecules at room temperature. Unlike many experiments and theoretical studies concentrating on the polaritonic response, we will mainly focus on how individual molecules (which are mostly composed of vibrational dark modes) relax and transfer energy under VSC. In detail, we will extensively study how vibrational energy relaxation and transfer depend on cavity mode detuning, molecular concentration (or Rabi splitting), and the number of hot molecules. Because there is no external polariton pumping, our investigation of how a cavity affects vibrational relaxation and energy transfer will hopefully yield insight into

[*] T. E. Li, Prof. Dr. A. Nitzan, Prof. Dr. J. E. Subotnik
Department of Chemistry, University of Pennsylvania
Philadelphia, Pennsylvania 19104 (USA)
E-mail: taoli@sas.upenn.edu
anitzan@sas.upenn.edu
subotnik@sas.upenn.edu
Prof. Dr. A. Nitzan
School of Chemistry, Tel Aviv University
Tel Aviv 69978 (Israel)

[**] A previous version of this manuscript has been deposited on a preprint server (https://arxiv.org/abs/2103.06749).

Supporting information and the ORCID identification number(s) for the author(s) of this article can be found under: https://doi.org/10.1002/anie.202103920.

the VSC modifications of individual molecular properties (such as chemical reaction rates) that are observed in experiments. In particular, by quantifying the asymptotic scaling of VSC effects with molecular system size or effective cavity volumes, our study will also partly address if VSC effects can persist and affect the properties of individual molecules in the limit that a very large number of molecules are present in a cavity.

The theoretical approach we will take is classical cavity molecular dynamics (CavMD) simulations,[14,17] a newly developed numerical tool implemented by the authors to classically propagate the coupled dynamics between realistic molecules (assumed to stay in their electronic ground-state) and cavity photons in the dipole gauge. Since the self-dipole term is included in the light-matter Hamiltonian of CavMD simulations, this numerical approach preserves gauge invariance and maintains numerical stability.[18] Compared with VSC experiments, this approach has reliably captured many VSC-induced phenomena, including an asymmetric Rabi splitting,[14,19] polariton relaxation to vibrational dark modes on a time scale of ps and sub-ps,[17,20] and a delay of population gain in the singly excited manifold of vibrational dark modes after pumping the lower polariton (LP), a process which stems from polariton enhanced molecular nonlinear absorption.[17,21] Hence, CavMD simulations appears to be a promising tool to study VSC-related phenomena.

A brief introduction of CavMD is given in SI Sec. I and II; see Ref. [17] for more details regarding CavMD simulations of a liquid CO_2 system and how the CO_2 force field is defined. In short, as shown in Figure 1, CavMD simulates a system with N_{sub} CO_2 molecules in a periodic cell coupled to a single cavity mode (with two polarization directions x and y). The effective coupling strength between each molecule and the cavity mode is $\tilde{\varepsilon}$. Note that, during nonequilibrium CavMD simulations, we have disregarded cavity loss. This simplification is valid because in Fabry–Pérot microcavities, the dominant channel for polaritons to relax is through vibrational dark modes (with a lifetime $\lesssim 1$ ps with our parameter setting[17]). By design cavity loss can take a longer lifetime (≈ 5 ps[16,20]). The effect of cavity loss on the reported results is discussed in SI Sec. V in detail. Below, we will report how VSC affects vibrational energy relaxation and transfer using CavMD simulations.

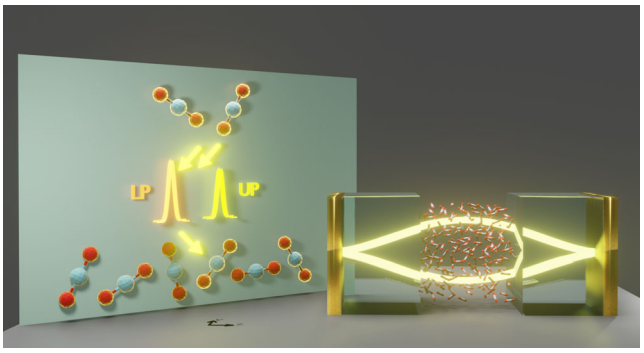

Figure 1. Sketch of the simulation setup where a large number of liquid-phase carbon dioxide molecules forms VSC with a single cavity mode. The left cartoon shows that the vibrational energy relaxation and transfer from hot (top) to thermal (bottom) molecules inside a cavity can be accelerated relative to that outside a cavity due to polariton-accelerated intermolecular vibrational energy transfer.

Results and Discussion

VSC Effects on Vibrational Energy Relaxation and Transfer

Figure 2a plots the IR spectrum outside the cavity (black line; $\tilde{\varepsilon}=0$) or inside the cavity (red line; $\tilde{\varepsilon}=2\times10^{-4}$ a.u.) when the cavity mode (at $\omega_c=2320\ cm^{-1}$; the dashed vertical blue line) forms VSC with the C=O asymmetric mode (peaked at $\omega_0=2327\ cm^{-1}$) of liquid CO_2. Inside the cavity, a pair of lower (LP; peaked at 2241 cm^{-1}) and upper (UP; peaked at 2428 cm^{-1}) polaritons form and these polaritons are separated by a Rabi splitting of 187 cm^{-1}. The IR spectrum is calculated by evaluating the Fourier transform of the dipole autocorrelation function from equilibrium trajectories; see SI Sec. III for details.

We now consider a nonequilibrium process where $N_{hot}=10$ uncorrelated hot molecules are immersed in a thermal CO_2 bath at room temperature (where in total there are $N_{sub}=216$ molecules in the simulation cell); see SI Sec. II for details. Figure 2b plots the average time-resolved C=O bond potential energy per hot molecule outside (black line) or inside (red line) the cavity, where a thermal energy $k_BT=300$ K has been subtracted from the C=O bond potential energy; note that here we use k_BT instead of $k_BT/2$ since each CO_2 molecule contains two C=O bonds. As shown in Figure 2b, the initial potential energy in the two C=O bonds per hot molecule is roughly $2\hbar\omega_c(\approx 6\times10^3$ K), i.e., the initial temperature of the hot molecules is $\approx 3\times10^3$ K. At later times, the vibrational energy relaxation of the hot molecules inside the cavity is accelerated compared with that outside the cavity. Meanwhile, as shown in Figure 2c, the average C=O bond potential energy per thermal molecule inside (red line) the cavity increases faster than that outside (black line) the cavity. Here, "thermal molecules" refer to molecules that were prepared at thermal equilibrium. During this nonequilibrium process, the total system energy is conserved: the simulation is performed under a NVE (constant number, volume, and energy) ensemble; see simulation details in SI Sec. I.

During the energy relaxation and transfer process, inside the cavity, Figure 2d plots the total (kinetic + potential) energy of the cavity photons ($\omega_c=2320\ cm^{-1}$ and with two polarization directions) subtracted by the thermal background $2k_BT$. Because cavity photons contribute half of the polaritons, Figure 2d indicates that polaritons can be transiently excited during this nonequilibrium process. Note that, at long times, the cavity photon energy does not decay back to zero because the relaxation of the hot molecules will increase the system temperature to above 300 K. From Figures 2b,c, we can conclude that the cavity acceleration of vibrational energy relaxation stems from cavity-accelerated intermolecular vibrational energy transfer from the hot to the thermal molecules. Furthermore, compared with thermal molecules (see Figure 2c red line), cavity photons can be excited more meaningfully at short times. This fact emphasizes the im-

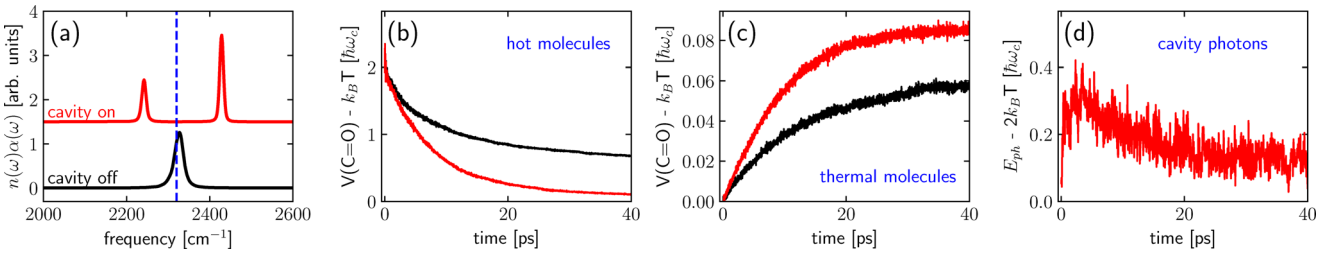

Figure 2. Rabi splitting and VSC effects on vibrational energy relaxation and transfer when $N_{sub}=216$ and $N_{hot}=10$. a) Simulated IR spectrum for liquid CO_2 outside (black) or inside (red) the cavity. For parameters, the cavity mode frequency is set to $\omega_c=2320\,cm^{-1}$ (denoted as the vertical blue line) and the effective coupling strength $\tilde{\varepsilon}=2\times10^{-4}$ a.u. (inside the cavity) or zero (outside the cavity). b,c) The corresponding average C=O bond potential energy (per molecule) dynamics for the hot (b) or thermal (c) molecules outside (black) or inside (red) the cavity. d) The corresponding photonic (kinetic + potential) energy dynamics inside the cavity, where two polarization directions of the cavity mode are taken into account. In the *y*-axis of (b–d), a thermal energy (i.e., k_BT for (b,c) and $2k_BT$ for (d)) has been subtracted and all energies are in units of $\hbar\omega_c$. See SI Sec. II for other simulation details. Note that polaritons play an important role during the process of vibrational energy relaxation and transfer as evidenced by the high transient photonic energy as compared with the vibrational energy transferred to the thermal molecules.

portance of forming polaritons and the interaction between polaritons and dark modes (which predominately constitute individual molecular properties) in modifying these rates.

In SI Sec. V, we show the effect of cavity loss on the results in Figures 2b–d. For most experiments of interest, including cavity loss has a negligible effect on vibrational relaxation; a modest cavity loss (1 ps lifetime) does not meaningfully alter energy transfer to thermal molecules, albeit a very fast cavity loss (100 fs lifetime) can greatly suppress the VSC effect on energy transfer and recover the outside-cavity result.

Detuning Dependence

Consider now the case where the cavity photon frequency is changed but all other parameters are the same as in Figure 2. Figure 3 plots the fitted vibrational energy relaxation rates of the hot molecules against the cavity mode detuning $\delta=\omega_c-\omega_0$. Note that in Figure 2b the outside-cavity decay curve (black line) suggests that the energy dissipation is not exactly exponential and the initial decay is faster than the later-time decay. By contrast, inside the cavity, since cavity photons can efficiently transfer energy from hot molecules to thermal molecules (both nearby *and* remote), the decay curve (red line) behaves more exponentially. In order to roughly quantify how (nonexponential) rates depend on detuning, in Figure 3 we use an exponential function $y=A\exp(-kt)$ to fit both the outside- and inside-cavity curves in a time interval 0–40 ps and obtain the overall effective decay rates. As shown in Figure 3, compared with the fitted decay rates outside the cavity (black squares), the rates inside the cavity (red circles) show a resonant dependence on the detuning δ: when $\delta\approx0$, the maximum rate inside the cavity is roughly four times the rate outside the cavity. Because the cavity mode is decoupled from the C=O asymmetric stretch under a large detuning, this resonance behavior again points to the importance of forming polaritons as far as modifying relaxation rates. As shown in SI Sec. VI, we have also found that the VSC effect on relaxation rates (which is calculated by taking the difference between the inside- versus outside-cavity rates) depends only weakly on the temperature of the hot molecules.

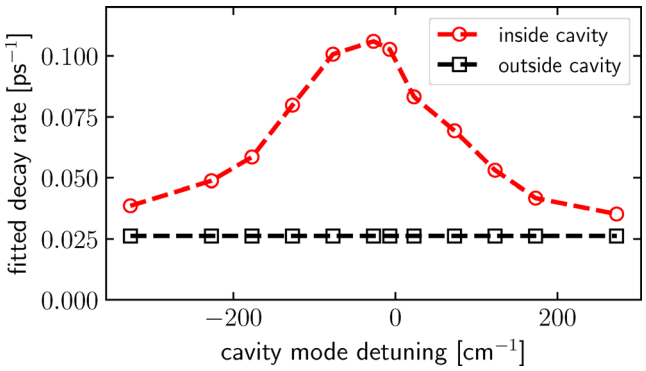

Figure 3. Fitted vibrational energy relaxation rates as a function of the cavity mode detuning. All parameters are the same as in Figure 2b except that we now change the cavity mode frequency (ω_c). Rates are obtained by fitting the signals in Figure 2b to a simple exponential function: $y=A\exp(-kt)$. Note that the VSC effect on vibrational energy relaxation resonantly depends on the cavity mode frequency.

Rabi Splitting Dependence

We next investigate how vibrational energy relaxation rates depend on the Rabi splitting by introducing an isotopic liquid mixture of carbon dioxide and changing the relative molecular concentration of each isotopic form. With all other parameters the same as Figure 2 (where a pure CO_2, i.e., $^{12}C^{16}O_2$ system is studied), Rabi splitting is tuned by replacing some $^{12}C^{16}O_2$ molecules by $^{14}C^{18}O_2$. Figure 4a plots the equilibrium IR spectrum inside the cavity under an increased concentration of $^{12}C^{16}O_2$ ($c=20\,\%$ to $100\,\%$ from bottom to top). Because $^{14}C^{18}O_2$ is relatively heavy, the $^{14}C{=}^{18}O$ asymmetric stretch (the leftest peak in Figure 4a) is well separated from the $^{12}C{=}^{16}O$ asymmetric stretch (peaked at $\omega_0=2327\,cm^{-1}$), and $^{14}C^{18}O_2$ molecules effectively do not participate in the formation of polaritons (LP and UP in Figure 4a) between the cavity mode (peaked at $2320\,cm^{-1}$) and the $^{12}C{=}^{16}O$ asymmetric stretch. The inset of Figure 4a plots the Rabi splitting Ω_N between the UP and LP as a function of $\sqrt{c/c_0}$, where $c_0=100\,\%$ denotes the concentration of pure $^{12}C^{16}O_2$. As in many experiments, a linear scaling between Ω_N and $\sqrt{c/c_0}$ is observed.

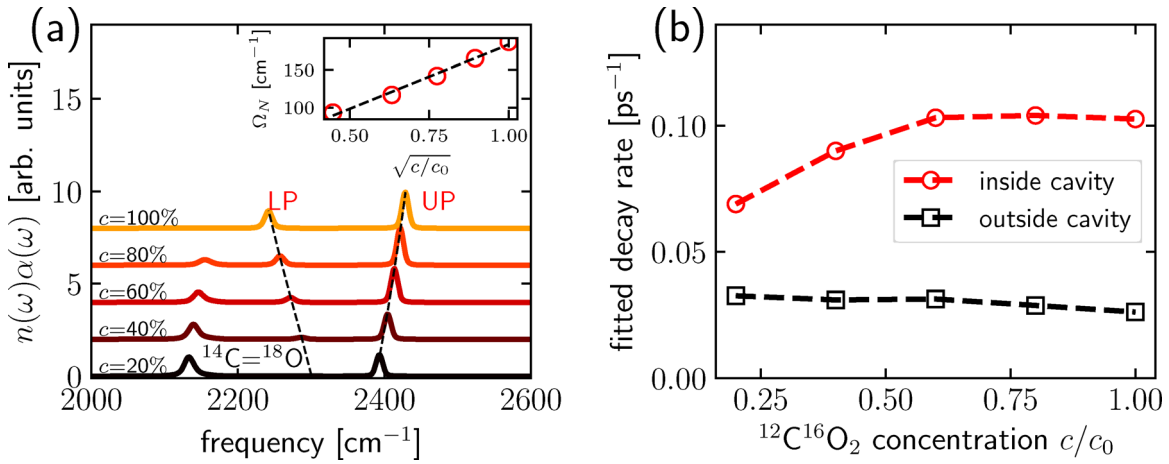

Figure 4. VSC effects on vibrational energy relaxation as a function of Rabi splitting. a) Simulated IR spectra for a liquid mixture of $^{12}C^{16}O_2$ and $^{14}C^{18}O_2$ inside the cavity. The cavity mode ($\omega_c = 2320\ cm^{-1}$) forms polaritons with the $^{12}C{=}^{16}O$ asymmetric stretch mode ($\omega_0 = 2327\ cm^{-1}$), while the $^{14}C{=}^{18}O$ asymmetric stretch mode (peak furthest to the left) is largely decoupled from the cavity. Note that when the $^{12}C^{16}O_2$ concentration increases from $c = 20\%$ to 100% (bottom to to top), the Rabi splitting (Ω_N) is also increased proportionally; see the inset. b) The corresponding fitted vibrational relaxation rates for the hot $^{12}C^{16}O_2$ molecules plotted against the $^{12}C^{16}O_2$ concentration (c/c_0), where $c_0 = 100\%$ denotes a pure $^{12}C^{16}O_2$ system. The rates inside the cavity (red circles) show a sensitive dependence on the $^{12}C^{16}O_2$ concentration (or Rabi splitting), while the rates outside the cavity (black squares) show a weak dependence on the concentration.

Under different concentrations of $^{12}C^{16}O_2$, Figure 4b plots the fitted vibrational energy relaxation rates when 10 hot $^{12}C^{16}O_2$ molecules ($N_{hot} = 10$) are immersed in the liquid mixture. The outside-cavity results (black squares) show a weak dependence on the molecular concentration. By contrast, inside the cavity (red circles), we observe an obvious acceleration of the relaxation rates when the $^{12}C^{16}O_2$ concentration is increased from $c = 20\%$ to 60% and then a plateau region above $c = 60\%$. This acceleration of the relaxation rates (with a monotonic dependence on molecular concentration) shows that, inside a cavity, the relaxation of a few molecules indeed depends strongly on the total molecular number (or concentration).

Interestingly, experiments outside a cavity[22] have shown that vibrational relaxation rates in hydrogen-bonded liquids (X-H/X-D mixture) depend sensitively on isotope concentration in a manner similar to what we have found inside a cavity in Figure 4b. In Ref. [22], the authors argued that such isotopic dependence can be explained by noting that, for a system with hydrogen bonding, intermolecular vibrational energy transfer can be facilitated by forming a delocalized intermediate state between two neighboring molecules. In an analogous pattern, Figure 4b implies that polaritons can similarly serve as a "delocalized intermediate state" and facilitate intermolecular vibrational energy transfer even in weakly interacting liquids.

Note, that in SI Sec. IV we show that, when Rabi splitting is enhanced by increasing the effective coupling strength $\tilde{\varepsilon}$ (instead of molecular concentration), the hot-molecule relaxation is also accelerated monotonically.

Superradiant-like Collective Relaxation

After demonstrating that VSC leads to cooperative effects on vibrational energy relaxation rates by investigating dependence on the molecular concentration or Rabi splitting, we next study how vibrational relaxation rates depend on the number of *hot* molecules (N_{hot}). Going beyond Figure 2 (where $N_{sub} = 216$ molecules are confined in a periodic simulation cell), here we simulate $N_{sub} = 2160$ molecules while keeping all other macroscopic variables—such as molecular density (1.101 g cm^{-3}) and the Rabi splitting—unchanged. Note that we maintain a constant Rabi splitting by reducing the effective light-matter coupling ($\tilde{\varepsilon}$) for each molecule. Physically speaking, increasing the number of molecules while adjusting the coupling so as to keeping the Rabi splitting constant corresponds to increasing the effective volume of the cavity at constant molecular density.

Figure 5a plots relaxation rates versus the number of hot molecules (N_{hot}) inside the large molecular system with $N_{sub} = 2160$. Both the inside- (red circles) and outside-cavity (black squares) rates show a reasonably linear relationship against N_{hot}. Outside the cavity, the linear scaling against N_{hot} is understandable because increasing the number of hot molecules increases the temperature of the system, enhances intermolecular collisions and strengthens dipole-dipole interactions, all of which can lead to an acceleration of the relaxation of hot molecules. More interestingly, the inside- and outside-cavity rates show different slopes against N_{hot}. The difference between these rates is plotted with green stars and represents a pure cavity effect. This pure cavity effect scales roughly linearly against N_{hot}, demonstrating that polariton-accelerated vibrational energy relaxation collectively depends on N_{hot}.

Another example demonstrating the collective behavior of vibrational relaxation is shown in Figure 5b, where we study the frequency distribution of the transiently excited photons (which effectively represents the polaritons). See SI Sec. III for details regarding the calculation of the polariton spectrum. As shown in Figure 5b, the polaritonic spectrum broadens (especially for the LP) and red-shifts when N_{hot}

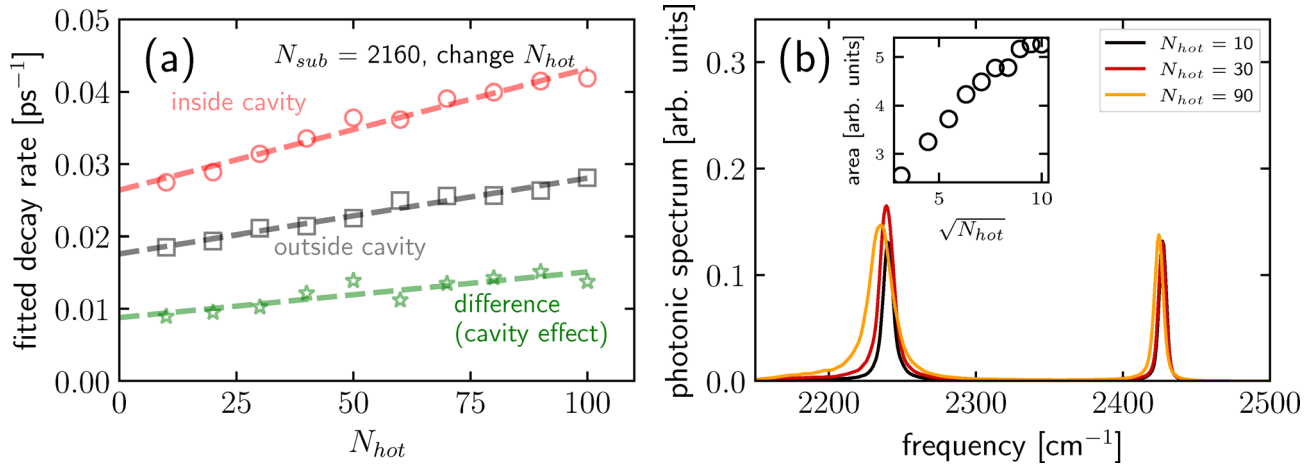

Figure 5. a) Fitted vibrational energy relaxation rates for the hot molecules inside (red circles) or outside (black squares) the cavity are plotted versus N_{hot}, with $N_{sub}=2160$ CO_2 molecules in the simulation cell. The difference between the inside- and outside-cavity results (green stars) is a pure VSC effect. Lines with different colors denote the respective linear fits of the rates. b) Corresponding transient photonic spectrum (which effectively represents a polaritonic spectrum) during the relaxation process when $N_{hot}=10$ (black), 30 (red), and 90 (orange). The inset plots the integrated area of the photonic spectrum versus $\sqrt{N_{hot}}$. Note that the intensity of the spectrum increases monotonically as the number of hot molecules increases. See SI Sec. II and III for simulation details and methods to calculate the transient spectrum.

increases [from $N_{hot}=10$ (black line) to $N_{hot}=90$ (orange line)]. In the inset of Figure 5b, we show that the total, integrated intensity of the polaritonic spectrum increases monotonically versus $\sqrt{N_{hot}}$. The polaritonic intensity gives a measure of the population of polaritonic states during this nonequilibrium relaxation process. The inset implies that when N_{hot} increases, the LP grows in intensity and can interact more strongly with the hot molecules in the system; the end result is an acceleration of the hot-molecule relaxation by what one might call polariton-enhanced decay. This collective behavior is reminiscent of the Dicke's superradiance phenomenon,[23] where the spontaneous emission rates of N electronic two-level systems can be collectively enhanced by a factor of N when all two-level systems interact with the same electromagnetic field. Here, we observe a similar behavior because all molecules interact with the same polaritons.

Asymptotic Scaling of System Size

Let us now address the asymptotic behavior of VSC effects for different molecular system sizes. Here, we change the number of molecules in the simulation cell (N_{sub}), while keeping the molecular density (1.101 g cm^{-3}) and the Rabi splitting the same. As mentioned above, this change corresponds to investigating different effective cavity volumes. As discussed in SI Sec. I, under these conditions (and especially the fixed Rabi splitting), second-order perturbative calculations suggest that the VSC effects on individual molecules should scale as $O(\tilde{\varepsilon}^2)=O(1/N_{sub})$. Below we will examine the scaling behavior for realistic CavMD simulations.

Standard O(1/N$_{sub}$) Scaling

When the simulation system is enlarged by increasing N_{sub} from 216 to 12960 and keeping the number of hot molecules ($N_{hot}=10$) fixed, Figure 6a plots the fitted average vibrational energy relaxation rates for the hot molecules inside (red circles) or outside (black squares) the cavity versus $1/N_{sub}$. Outside the cavity, the rates decrease when N_{sub} increases until converging to a plateau regime ($1/N_{sub}<0.002$), which corresponds to the limit when every hot molecule dissipates its energy separately in an infinite thermal bath. This observation is understandable because increasing the system size while keeping $N_{hot}=10$ effectively decreases the temperature of the system and suppresses the relaxation rate, which is consistent with the outside-cavity scaling in Figure 5a. More importantly, the difference between the inside- and outside-cavity rates—which is a pure VSC effect—scales linearly with $1/N_{sub}$, which confirms the standard perturbative result. Also as shown in Figure 6b (inset), when N_{sub} increases, the intensity of the polaritonic spectrum decreases as the transient polaritonic spectrum converges to the spectrum under thermal equilibrium (e.g., Figure 2a). This decrease arises because under a fixed Rabi splitting, the light-matter coupling $\tilde{\varepsilon}$ for each molecule decreases when N_{sub} increases, thus leading to a negligible polaritonic effect on the relaxation rates for the hot molecules.

Slower-than-O(1/N$_{sub}$) Scaling

Rather than studying VSC with a fixed number of hot molecules ($N_{hot}=10$) and a variable number of molecules in a simulation cell (N_{sub}), another approach is to keep fixed $N_{hot}/N_{sub}=10/216=4.63\,\%$. This approach captures the physical reality that, as extensive properties, both N_{hot} and N_{sub} should scale proportional to one another as a function of system size. In Figure 6c, we plot vibrational energy relaxation rates for the hot molecules with different N_{sub}. Here, the outside-cavity rate (black squares) is independent of the system size. In other words, the rate is an extensive property versus the system size, suggesting that increasing N_{hot} and N_{sub} at the same time is a more appropriate approach for studying the system size dependence than keeping $N_{hot}=10$ fixed (as

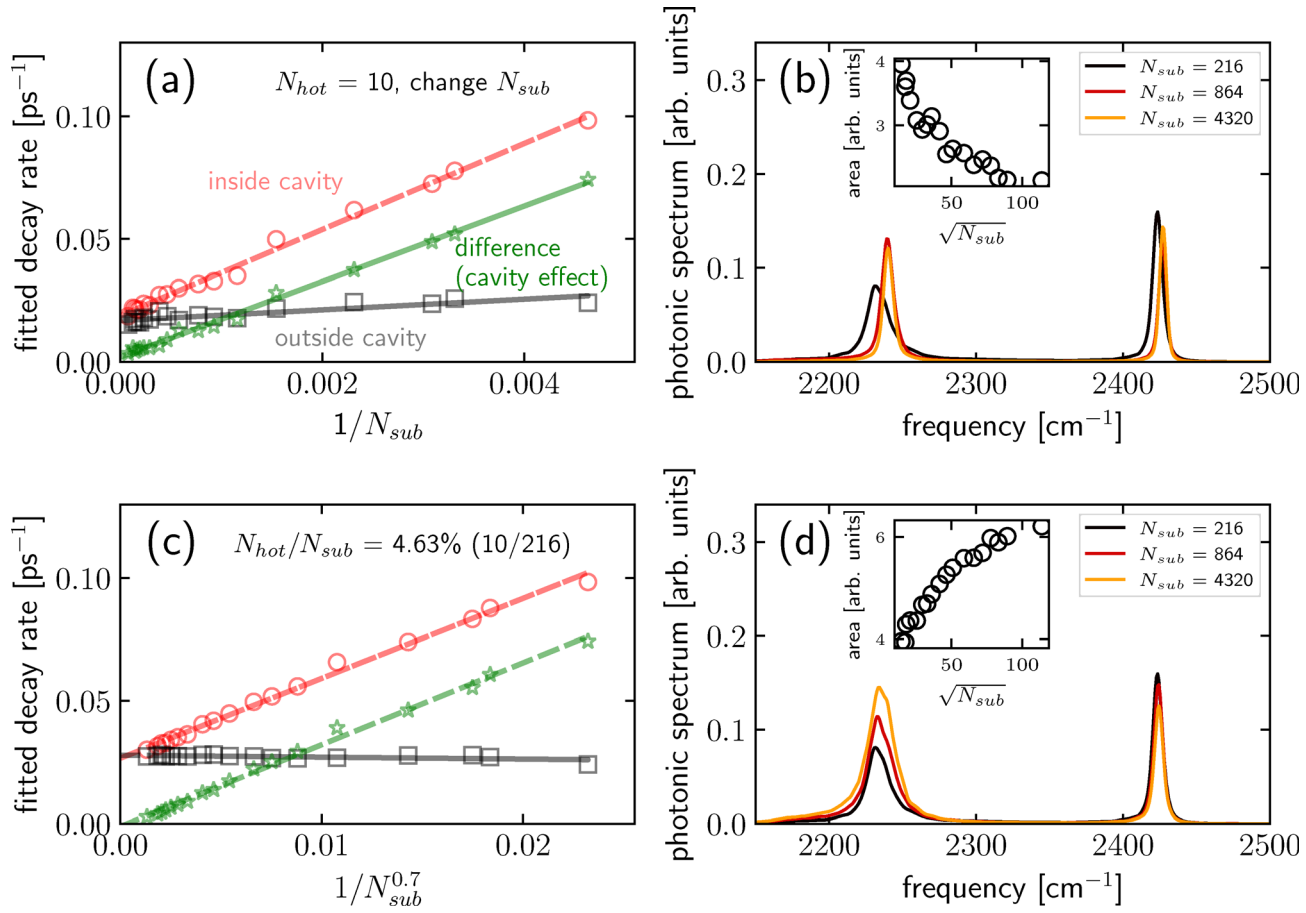

Figure 6. The dependence of vibrational energy relaxation rates on molecular system size (N_{sub}). a) Fitted vibrational energy relaxation rates for the hot molecules inside (red circles) or outside (black squares) the cavity against $1/N_{sub}$ when $N_{hot}=10$ is fixed. We observe a linear scaling between the difference (green stars), which is a pure VSC effect, and $1/N_{sub}$. b) Corresponding transient polaritonic spectrum for the different molecular system sizes in (a): $N_{sub}=216$ (black), 864 (red), and 4320 (orange). The inset plots the integrated area of the photonic spectrum versus $\sqrt{N_{sub}}$. c) Fitted vibrational energy relaxation rates for the hot molecules against $1/N_{sub}^{0.7}$ when $N_{hot}/N_{sub}=10/216=4.63\,\%$. d) The transient polaritonic spectrum corresponding to the different molecular system sizes in (c); the inset in (d) corresponds the inset in (b) as well.

above). If we compare the inside- and outside-cavity rates, the average cavity effect (green stars) on vibrational energy relaxation rates remains meaningful (i.e., $>10\,\%$ cavity effect compared with the rates outside the cavity) even when N_{sub} reaches up to $\sim 10^4$. For example, when $N_{sub}=8\times10^3$, the cavity effect on the relaxation rates is 0.004 ps^{-1}, which is 14 % of the bare relaxation rate (0.028 ps^{-1}) outside the cavity.

The most interesting feature of Figure 6c is that the cavity effect scales with $1/N_{sub}^{0.7}$ (instead of $1/N_{sub}$); see lines with different colors which represent linear fits of the corresponding rates versus $1/N_{sub}^{0.7}$. Here, we note that the 0.7 in the exponent should not be regarded as a universal quantity and might vary by changing simulation parameters (e.g. the ratio N_{hot}/N_{sub}). The underlying mechanism behind this nontrivial slower-than-$O(1/N_{sub})$ scaling comes from the opposing effects of the reduced light-matter coupling $\tilde{\varepsilon}$ and the increased number of hot molecules (N_{hot}) that arises when N_{sub} increases. On the one hand, when $\tilde{\varepsilon}$ decreases proportionally to $1/\sqrt{N_{sub}}$, as mentioned below Figure 6a, the cavity effect on vibrational energy relaxation rates tends to exhibit an $O(1/N_{sub})$ scaling. On the other hand, according to Figure 6d where we plot the corresponding polaritonic spectrum for different molecular system sizes, the transiently excited LP intensifies for larger molecular systems (which is similar to Figure 5b). Hence, this intensified LP tends to accelerate the vibrational relaxation when N_{hot} increases. Overall, these two competing effects lead to a slower-than-$O(1/N_{sub})$ scaling.

A recent experimental work[24] shows that the observed vibrational relaxation rate of the "dark reservoir" (or the hot molecules) is not modified in a Fabry–Pérot microcavity (where the molecular number can reach $10^9\sim10^{12}$), which is consistent with our simulation results. For plasmonic cavities—an emerging platform for studying VSC,[25,26] since the effective cavity volume is much less than Fabry–Pérot microcavities, the slower-than-$O(1/N_{sub})$ scaling could be observed in experiments.

Polaritonic Energy Redistribution

Another interesting and potentially significant observation is the way transiently excited polaritons redistribute their energy among molecules following the vibrational energy relaxation process. For the same conditions as in Figures 6c,d, Figure 7a plots the logarithmic-scaled density distribution of

the C=O bond potential energy (in unit of $\hbar\omega_0$, where $\omega_0 = 2327\ cm^{-1}$) for the molecules prepared at thermal equilibrium (or "thermal molecules"). For this calculations, we set $N_{sub} = 2000$ and run 40 NVE nonequilibrium trajectories; for each trajectory we calculate the energy distribution by taking snapshots every 1 ps during the 40-ps simulation, so that overall we count $40 \times 40 \times 2000$ CO_2 configurations during the whole relaxation and transfer process. During this time, both the outside (cyan bins) and inside (purple bins) cavity results demonstrate an exponential distribution, which implies that the C=O bond potential energy of thermal molecules roughly obey a Maxwell-Boltzmann distribution; recall that the *y*-axis is on a logarithmic scale. Very interestingly, however, the tail of the distributions of C=O vibrational energy differ strongly inside versus outside the cavity. This fact is more clearly shown in Figure 7b which plots the ratio of the probability density of thermal-molecule C=O bond potential energy inside versus outside the cavity (the bins in Figure 7a). Because both simulations start from exactly the same initial conditions and with $\tilde{\varepsilon}$ switched on or off (see SI Sec. II for details), this difference in the tail distribution is a pure polaritonic effect, i.e., the transiently excited polaritons are more likely to create vibrationally higher excited molecules rather than equally distributing energy to all thermal molecules.

A possible explanation for the large difference in the tail could come from the perspective of spectral overlap between polaritons and dark modes (which predominately constitutes individual molecular properties). Due to anharmonicity, the molecules at the tail of energy distribution have smaller vibrational frequencies, leading to a larger spectral overlap with the LP. Therefore, the transiently excited LP would interact more strongly with the molecules at the tail and transfer more energy to these molecules than molecules with small vibrational energy.

Finally, we remark that, since this polaritonic effect mostly takes place in the long tail of the thermal molecule C=O vibrational energy distribution, it is possible that polariton-accelerated vibrational energy transfer may still be meaningful for a small subset of thermal molecules even when N_{sub} is very large. In other words, event though the average VSC effects per molecule will vanish once N_{sub} exceeds $\sim 10^4$ (see Figure 6), some molecules in the tail of the distribution may feel the effect of the polaritons when N_{sub} is beyond $\sim 10^4$ (i.e., in larger volume cavities). Future work will investigate this possibility.

Conclusion

We have studied the effect of VSC on vibrational energy relaxation and transfer for a small fraction of hot molecules immersed in a thermal bath of CO_2 at room temperature. Several important observations have been made: (i) During this nonequilibrium process with no external pumping, polaritons (especially the LP) can be transiently excited and facilitate intermolecular vibrational energy transfer, which leads to an acceleration of vibrational energy relaxation of the hot molecules. (ii) This acceleration resonantly depends on the cavity mode detuning and can be enhanced by increasing Rabi splitting (or molecular concentration). (iii) The vibrational relaxation acceleration is superradiant-like and collectively scales with the number of hot molecules. (iv) For large system sizes (or large effective cavity volumes), when the fraction between the number of hot and thermal molecules remains the same, the VSC effect on the relaxation rates scales slower than $1/N_{sub}$ due to a competition between the reduced light-matter coupling ($\tilde{\varepsilon}$) and an enhanced superradiant-like behavior of the hot molecules. (v) Although our simulations suggest that the effect of VSC on the average relaxation rates becomes negligible when N_{sub} exceeds $\sim 10^4$, polaritons are always transiently and meaningfully excited, and the energy infused into the polaritons transfers more strongly to the tail of the thermal-molecule energy distribution. Altogether, this work suggests that collective VSC effects in a cavity can significantly affect vibrational relaxation energy relaxation and transfer. Note that, in order to arrive at these conclusions, analyzing transient polaritonic motion and energy distribution, we had to use a realistic molecular dynamic model in which thermal molecular

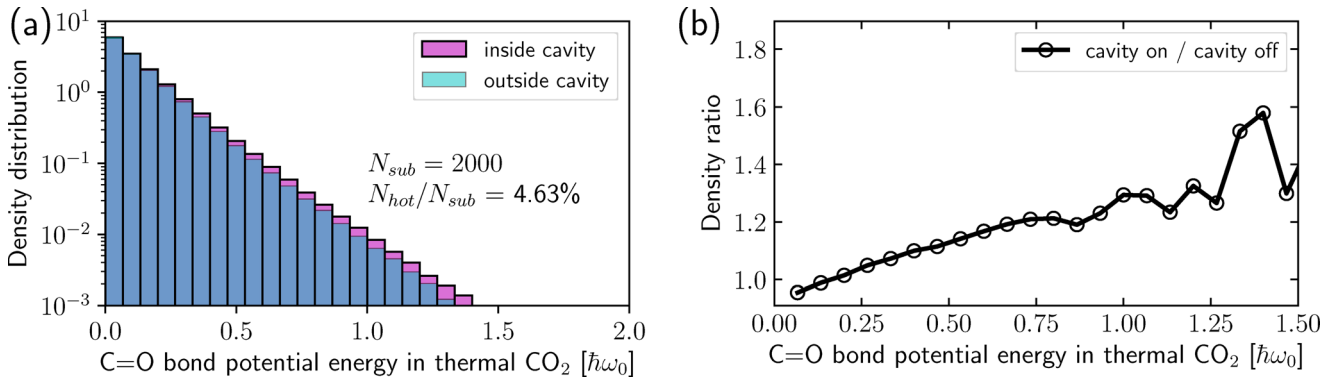

Figure 7. a) Logarithmic-scaled density distribution of the C=O bond potential energy as found in the molecules prepared in thermal equilibrium ("thermal molecules") during the hot-molecule relaxation process. We fix $N_{sub} = 2000$ and $N_{hot}/N_{sub} = 4.63\%$. Purple bins denote the inside-cavity results. Cyan bins denote the outside-cavity results, which are barely observed in the figure because the inside- and outside-cavity distributions largely overlap with each other (the overlap of purple and cyan is blue). b) The corresponding density ratio between the inside- versus outside-cavity distribution of C=O bond potential energy. Note that the polaritons prefer to transfer energy to a small subset of thermal molecules located at the tail of the distribution.

motions and intermolecular interactions lead to evolving molecular disorder and vibrational disorder.

Finally, let us make a few remarks regarding the connection of this work to VSC catalytic effects on ground-state chemical reactions observed in Fabry–Pérot microcavities. The rates of vibrational energy relaxation and transfer can significantly modify ground-state chemical reaction rates outside the cavity. For example, Kramers' theory[27,28] suggests that ground-state reaction rates can depend proportionally or inversely on the energy relaxation rate. Therefore, the observation of VSC effects on vibrational energy relaxation and transfer might imply the modification of ground-state chemical reaction rates. That being said, VSC catalysis is highly nontrivial as experiments suggest (at least) the following four criteria.[3,4,6] (i) The chemical reaction rates are modified under thermal conditions and without external polaritonic pumping. The cavity modification of chemical reaction rates (ii) resonantly depends on the cavity mode detuning and (iii) collectively depends on molecular concentration (or Rabi splitting). (iv) The cavity modification can be observed in Fabry–Pérot microcavities (where the effective cavity volume is $\sim\lambda^3$ and λ takes units of micrometers), meaning that the number of molecules forming VSC can reach $10^9 \sim 10^{12}$. As far as understanding VSC effects by studying vibrational energy relaxation and transfer, the results presented here are consistent with criteria (i)–(iii). However, when criterion (iv) (the number limit) is considered, we have observed a negligible average VSC effect per molecule once N_{sub} exceeds $\sim 10^4$. That being said, our simulation suggests a larger polaritonic effect for molecules at the tail of the energy distribution. Because chemical reactions also occur at this same tail, such a similarity indicates that VSC effects on vibrational energy relaxation and transfer could possibly play a significant role in VSC catalysis—a hypothetical premise that deserves further study.

Acknowledgements

This material is based upon work supported by the U.S. National Science Foundation under Grant No. CHE1953701 (A.N.); and the U.S. Department of Energy, Office of Science, Basic Energy Sciences, Chemical Sciences, Geosciences, and Biosciences Division (J.E.S.).

Conflict of interest

The authors declare no conflict of interest.

Keywords: energy transfer · molecular dynamics · vibrational relaxation · vibrational strong coupling

[1] J. George, A. Shalabney, J. A. Hutchison, C. Genet, T. W. Ebbesen, *J. Phys. Chem. Lett.* **2015**, *6*, 1027 – 1031.
[2] J. George, T. Chervy, A. Shalabney, E. Devaux, H. Hiura, C. Genet, T. W. Ebbesen, *Phys. Rev. Lett.* **2016**, *117*, 153601.
[3] A. Thomas, J. George, A. Shalabney, M. Dryzhakov, S. J. Varma, J. Moran, T. Chervy, X. Zhong, E. Devaux, C. Genet, J. A. Hutchison, T. W. Ebbesen, *Angew. Chem. Int. Ed.* **2016**, *55*, 11462 – 11466; *Angew. Chem.* **2016**, *128*, 11634 – 11638.
[4] A. Thomas, A. Jayachandran, L. Lethuillier-Karl, R. M. Vergauwe, K. Nagarajan, E. Devaux, C. Genet, J. Moran, T. W. Ebbesen, *Nanophoton.* **2019**, *9*, 249 – 255.
[5] A. Thomas, L. Lethuillier-Karl, K. Nagarajan, R. M. A. Vergauwe, J. George, T. Chervy, A. Shalabney, E. Devaux, C. Genet, J. Moran, T. W. Ebbesen, *Science* **2019**, *363*, 615 – 619.
[6] J. Lather, P. Bhatt, A. Thomas, T. W. Ebbesen, J. George, *Angew. Chem. Int. Ed.* **2019**, *58*, 10635 – 10638; *Angew. Chem.* **2019**, *131*, 10745 – 10748.
[7] K. Hirai, H. Ishikawa, J. Hutchison, H. Uji-i, *ChemRxiv* **2020**, https://doi.org/10.26434/chemrxiv.13191617.v1.
[8] J. Galego, C. Climent, F. J. Garcia-Vidal, J. Feist, *Phys. Rev. X* **2019**, *9*, 021057.
[9] J. A. Campos-Gonzalez-Angulo, R. F. Ribeiro, J. Yuen-Zhou, *Nat. Commun.* **2019**, *10*, 4685.
[10] T. E. Li, A. Nitzan, J. E. Subotnik, *J. Chem. Phys.* **2020**, *152*, 234107.
[11] J. A. Campos-Gonzalez-Angulo, J. Yuen-Zhou, *J. Chem. Phys.* **2020**, *152*, 161101.
[12] D. Sidler, C. Schäfer, M. Ruggenthaler, A. Rubio, *J. Phys. Chem. Lett.* **2021**, *12*, 508 – 516.
[13] X. Li, A. Mandal, P. Huo, *Nat. Commun.* **2021**, *12*, 1315.
[14] T. E. Li, J. E. Subotnik, A. Nitzan, *Proc. Natl. Acad. Sci. USA* **2020**, *117*, 18324 – 18331.
[15] M. Gruebele, P. G. Wolynes, *Acc. Chem. Res.* **2004**, *37*, 261 – 267.
[16] B. Xiang, R. F. Ribeiro, M. Du, L. Chen, Z. Yang, J. Wang, J. Yuen-Zhou, W. Xiong, *Science* **2020**, *368*, 665 – 667.
[17] T. E. Li, A. Nitzan, J. E. Subotnik, *J. Chem. Phys.* **2021**, *154*, 094124.
[18] C. Schäfer, M. Ruggenthaler, V. Rokaj, A. Rubio, *ACS Photonics* **2020**, *7*, 975 – 990.
[19] R. M. A. Vergauwe, A. Thomas, K. Nagarajan, A. Shalabney, J. George, T. Chervy, M. Seidel, E. Devaux, V. Torbeev, T. W. Ebbesen, *Angew. Chem. Int. Ed.* **2019**, *58*, 15324 – 15328; *Angew. Chem.* **2019**, *131*, 15468 – 15472.
[20] B. Xiang, R. F. Ribeiro, A. D. Dunkelberger, J. Wang, Y. Li, B. S. Simpkins, J. C. Owrutsky, J. Yuen-Zhou, W. Xiong, *Proc. Natl. Acad. Sci. USA* **2018**, *115*, 4845 – 4850.
[21] B. Xiang, R. F. Ribeiro, L. Chen, J. Wang, M. Du, J. Yuen-Zhou, W. Xiong, *J. Phys. Chem. A* **2019**, *123*, 5918 – 5927.
[22] D. J. Shaw, M. R. Panman, S. Woutersen, *Phys. Rev. Lett.* **2009**, *103*, 227401.
[23] R. H. Dicke, *Phys. Rev.* **1954**, *93*, 99 – 110.
[24] A. B. Grafton, A. D. Dunkelberger, B. S. Simpkins, J. F. Triana, F. J. Hernández, F. Herrera, J. C. Owrutsky, *Nat. Commun.* **2021**, *12*, 214.
[25] Z. T. Brawley, S. D. Storm, D. A. Contreras Mora, M. Pelton, M. Sheldon, *J. Chem. Phys.* **2021**, *154*, 104305.
[26] D. Yoo, F. de León-Pérez, M. Pelton, I.-H. Lee, D. A. Mohr, M. B. Raschke, J. D. Caldwell, L. Martín-Moreno, S.-H. Oh, *Nat. Photonics* **2021**, *15*, 125 – 130.
[27] H. Kramers, *Physica* **1940**, *7*, 284 – 304.
[28] A. Nitzan, *Chemical Dynamics in Condensed Phases: Relaxation, Transfer and Reactions in Condensed Molecular Systems*, Oxford University Press, New York, **2006**.

Manuscript received: March 18, 2021
Accepted manuscript online: May 6, 2021
Version of record online: ■■ ■■, ■■■■

Research Articles

Vibrational Strong Coupling

T. E. Li,* A. Nitzan,*
J. E. Subotnik* _____ ▮▮▮▮–▮▮▮▮

Collective Vibrational Strong Coupling Effects on Molecular Vibrational Relaxation and Energy Transfer: Numerical Insights via Cavity Molecular Dynamics Simulations

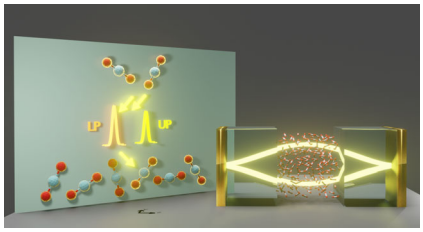

We performed cavity molecular dynamics simulations and showed that, under vibrational strong coupling conditions, vibrational relaxation and energy transfer from hot to thermal molecules can be accelerated relative to that outside a cavity due to polariton-accelerated intermolecular vibrational energy transfer.